8.6 RELATIVE STABILITY OF HELIUM AND HYDROGEN IN NANO-STRUCTURED FERRITIC ALLOYS — B. Tsuchiya, T. Yamamoto, G. R. Odette, (University of California, Santa Barbara); K. Ohsawa (Kyushu University)

OBJECTIVE

Ab-initio Density Functional Theory (DFT) calculations were carried out to assess the energies of He and H at various locations in $Y_2Ti_2O_7$ and compared the corresponding energies in matrix Fe.

SUMMARY

First principle calculations were carried out for tetrahedral- and octahedral-interstitial sites in $Y_2Ti_2O_7$, and tetrahedral- and octahedral-interstitial as well as substitutional sites in Fe, in order to assess the energetics of He and H in Fe containing $Y_2Ti_2O_7$. The formation energies of He at tetrahedral- and octahedral-interstitial sites in $Y_2Ti_2O_7$ were 1.59 and 1.02 eV, respectively, which were much lower than the corresponding energies (4.47, 4.67, and 2.23 eV) in tetrahedral-, octahedral-interstitial and substitutional sites in Fe. On the other hand, the formation energies of H at tetrahedral- and octahedral-interstitial sites in $Y_2Ti_2O_7$ were 2.87 and 3.01 eV, respectively, which are much higher than the corresponding energies (0.11, 0.24, and 0.41 eV) at tetrahedral-, octahedral-interstitial and substitutional sites in Fe. Thus He and H in NFAs partition to the oxide and Fe, respectively.

PROGRESS AND STATUS

Introduction

Nano-structured ferritic alloys (NFAs), containing a very high density of nanometer-sized pyrochlore-type Y-Ti-O oxide ($Y_2Ti_2O_7$) nanofeatures (NFs), are a leading candidate structural material for advanced fission and fusion energy applications [1-3]. The oxide particles act as obstacles for dislocation motion, increasing the alloy strength, and are expected to act as recombination centers for point defects and trapping sites for helium (He) atoms that are produced by nuclear transmutation reactions to restrain the swelling. Our results confirm and extend previous first principal studies that He prefers substitutional sites in bcc iron (Fe) and individual octahedral-interstitial sites in $Y_2Ti_2O_7$ [4, 5]. Thus the oxides are sites for bubble formation that largely suppress swelling [2]. In this work we also extend the assessment of site-specific energies to hydrogen (H).

Calculation Methods

Figure 1 shows configurations of the ideal pyrochlore-type $Y_2Ti_2O_7$ with lattice constants of 0.9974 nm for a, b, and c axes. The structure has an isometric with space group of $Fd\bar{3}m$: 227 and possess eight molecules consisting of 16 pieces of Y^{3+} cations, 16 pieces of Ti^{4+} cations, and 56 (=48+8) pieces of O^{2-} anions in the unit cell (16+16+56=88 cations and anions; large size of the unit cell). Each cation and anion in the conventional cell locate at the following Wyckoff positions: Y^{3+} at 16*d* (1/2, 1/2, 1/2), Ti^{4+} at 16*c* (0, 0, 0), O^{2-} at 48*f* (*x*, 1/8, 1/8) in a tetrahedron coordinated to two Y^{3+} and two Ti^{4+} cations and at 8*b* (3/8, 3/8, 3/8) in a tetrahedron formed by four Y^{3+} cations, where the displacement of each O-site due to the neighboring unoccupied tetrahedron formed by four Ti^{3+} cations, *x*, is the only internal free parameter [2, 6]. Figure 2 shows configurations of Fe bulk having body-center cubic (bcc) crystal structure with lattice constants of 0.2842 nm for a, b, and c axes and space group of $Im\bar{3}m$: 229 and containing 128 pieces of Fe^{4+} cations in the supercell [2, 4, 7-13]. The Fe^{4+} cations locate at the Wyckoff position of 2*a* (0, 0, 0). All structural relaxations and energetic calculations were carried out using periodic primitive cells and supercells, the DFT code – VASP ver. 4.6, a plane-wave basis generated with valence configurations of H-$1s^1$, He-$1s^2$, O-$2s^22p^4$, Ti-$3s^23p^63d^24s^2$, Fe-$3d^64s^2$, and Y-$4s^24p^64d^15s^2$ and the projector augmented wave method (PAW) [14, 15]. One He or H atom was inserted in the center of (a) tetrahedron and (b) octahedron, surrounded by four Ti atoms and three Y and three Ti atoms, respectively, in bulk $Y_2Ti_2O_7$, as shown in Fig. 1. The energy cutoff was set at 650 eV for He and 500 eV for H and a 5×5×5 Monkhorst-Pack k-mesh was used for the unit $Y_2Ti_2O_7$ cell, because of approximately 1.5 times as much as maximal plane-wave kinetic energy (e.g; 479 eV for He, 400 eV for O, 275 eV for Ti, 250 eV for H, 212 eV for Y). The period of the first principal calculation was 24 hrs for the oxide and

the three rounds was carried out to obtain the values. On the other hand, it was also shown in Fig. 2 that various defect structures, including interstitial He and H at tetrahedral- and octahedral-interstitial sites, a He or H atom occupying a Fe vacancy site (i.e. substitutional He or H) were modeled. The energy cutoff was set at 350 eV for He and H and 7×7×7 Monkhorst-Pack k-mesh was used for Fe in its 4×4×4 bcc supercells. The calculation for 120 hrs was repeated until three rounds. Spin-polarised calculations were performed for Fe and non-spin-polarised calculations in the case of $Y_2Ti_2O_7$.

The formation energies of He and H defects at interstitial sites in $Y_2Ti_2O_7$, $E_{\text{defect}}^{\text{He in Y}_2\text{Ti}_2\text{O}_7}$ and $E_{\text{defect}}^{\text{H in Y}_2\text{Ti}_2\text{O}_7}$, are defined, as given in Eqs. (1) and (2).

$$E_{\text{defect}}^{\text{He in Y}_2\text{Ti}_2\text{O}_7} = E_{\text{He in Y}_2\text{Ti}_2\text{O}_7} - E_{\text{Y}_2\text{Ti}_2\text{O}_7} - E_{\text{He}}, \quad (1)$$

$$E_{\text{defect}}^{\text{H in Y}_2\text{Ti}_2\text{O}_7} = E_{\text{H in Y}_2\text{Ti}_2\text{O}_7} - E_{\text{Y}_2\text{Ti}_2\text{O}_7} - E_{\text{H}_2}/2, \quad (2)$$

where $E_{\text{He in Y}_2\text{Ti}_2\text{O}_7}$, $E_{\text{H in Y}_2\text{Ti}_2\text{O}_7}$, and $E_{\text{Y}_2\text{Ti}_2\text{O}_7}$ are the total energies of the He- and H-doped defective and defect-free unit $Y_2Ti_2O_7$ cells, respectively, that consist of 16 Y, 16 Ti, and 56 O atoms. E_{He} and E_{H_2} represent the total energies (E_{He}=-0.000448 eV/formula unit, E_{H_2}=-6.7449 eV/formula unit) of a cubic box with 1 nm sides that contains an isolated He atom and gaseous hydrogen molecule (H_2), respectively, which have been calculated using the energy cutoffs of 650 eV for He and 350 eV for H and 1×1×1 Monkhorst-Pack k-mesh. As denoted at the third term of Eq. (2), it was assumed that half the total energy of H_2 indicated to the total energy of an isolated H atom, $E_{\text{H}} = E_{\text{H}_2}/2$ =-3.3725 eV/atom, which corresponded to the calculated binding energy of the H_2/2 molecule [13, 16]. The bond length of H_2 was calculated to be 0.0751 nm, which was in fairly good agreement with the other calculated (0.0750 nm) [8] and experimental data (0.0741 nm) [17]. Similarly, the formation energies of substitutional He and H in Fe, $E_{\text{defect}}^{\text{He in Fe}}$ and $E_{\text{defect}}^{\text{H in Fe}}$, are defined in the same manner as follows;

$$E_{\text{defect}}^{\text{He in Fe}} = E_{\text{He in Fe}} - E_{\text{Fe}} - E_{\text{He}}, \quad (3)$$

$$E_{\text{defect}}^{\text{H in Fe}} = E_{\text{H in Fe}} - E_{\text{Fe}} - E_{\text{H}_2}/2, \quad (4)$$

where $E_{\text{He in Fe}}$, $E_{\text{H in Fe}}$, and E_{Fe} are the total energies of the He- and H-doped defective and defect-free supercells that consist of 128 Fe atoms, respectively. In addition, the defect formation energies of He- and H-occupying Fe-vacancy sites, $E_{\text{defect}}^{\text{He}}$ and $E_{\text{defect}}^{\text{H}}$, are defined in the same manner as follows:

$$\begin{aligned} E_{\text{defect}}^{\text{He}} &= E_{\text{defect}}^{\text{He+V}} - E_{\text{defect}}^{\text{V}} \\ &= \left(E_{\text{He+V in Fe}} - mE_{\text{Fe}}/128 - E_{\text{He}}\right) - \left(E_{\text{V in Fe}} - mE_{\text{Fe}}/128\right) \\ &= E_{\text{He+V in Fe}} - E_{\text{V in Fe}} - E_{\text{He}}, \end{aligned} \quad (5)$$

$$\begin{aligned} E_{\text{defect}}^{\text{H}} &= E_{\text{defect}}^{\text{H+V}} - E_{\text{defect}}^{\text{V}} \\ &= \left(E_{\text{H+V in Fe}} - mE_{\text{Fe}}/128 - E_{\text{H}_2}/2\right) - \left(E_{\text{V in Fe}} - mE_{\text{Fe}}/128\right) \\ &= E_{\text{He+V in Fe}} - E_{\text{V in Fe}} - E_{\text{H}_2}/2, \end{aligned} \quad (6)$$

where $E_{\text{defect}}^{\text{V}}$ and $E_{\text{V in Fe}}$ are the formation and total, respectively, energies of a vacancy in Fe bulk, and $E_{\text{defect}}^{\text{He+V}}$ is the addition of $E_{\text{defect}}^{\text{He}}$ to $E_{\text{defect}}^{\text{V}}$. $E_{\text{He+V in Fe}}$ and $E_{\text{H+V in Fe}}$ are the total energies of the defective supercells that include each one He and H atom with *m* Fe atoms, *m*=127.

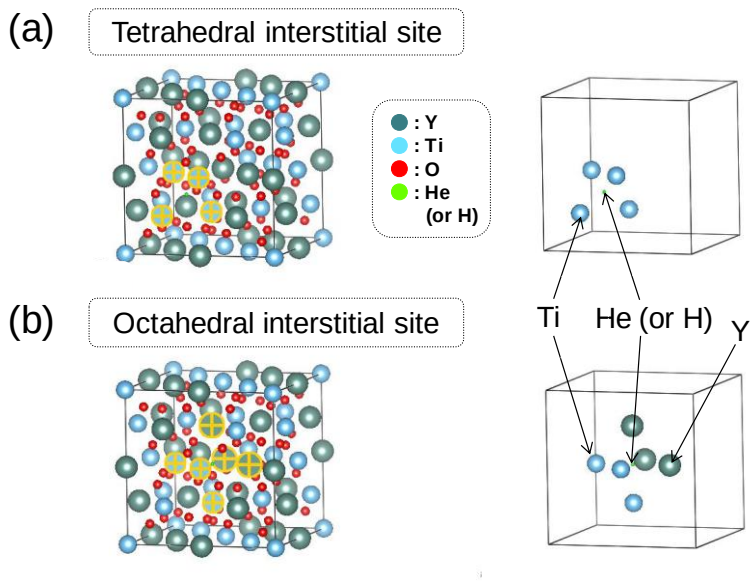

Figure 1. Configurations of various He and H in (a) tetrahedral- and (b) octahedral-interstitial sites surrounded by four Ti^{4+} cations and three Y^{3+} and three Ti^{4+} cations, respectively, in bulk $Y_2Ti_2O_7$.

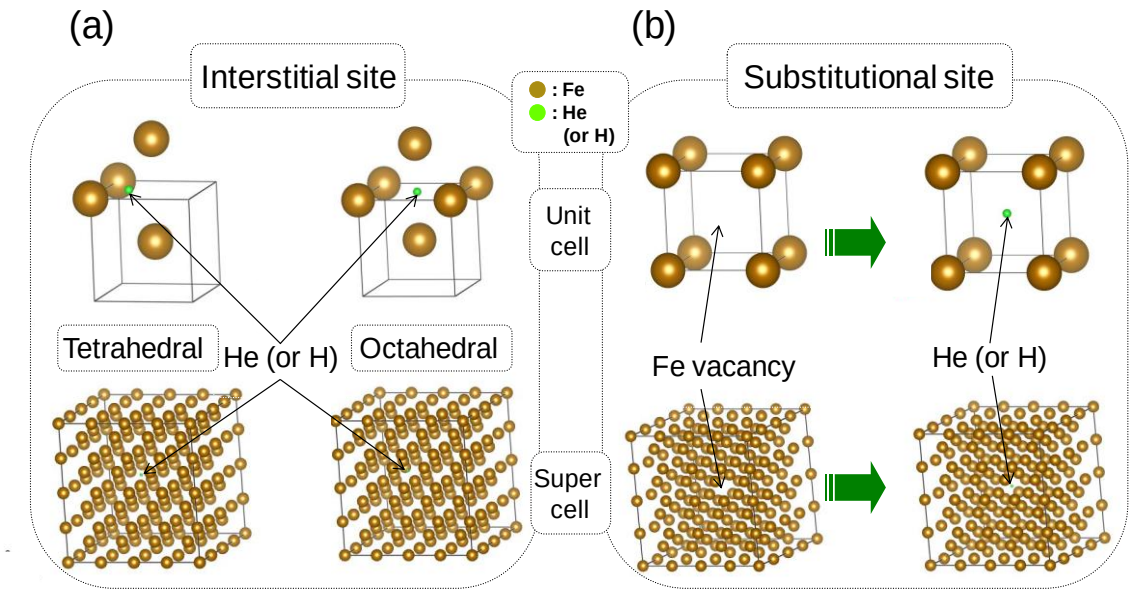

Figure 2. Configurations of various He and H in (a) tetrahedral- and octahedral-interstitial sites and (b) a Fe vacancy (substitutional site).

Results and Discussion

Figure 3 shows calculated formation energies of He and H in tetrahedral- and octahedral-interstitial sites in $Y_2Ti_2O_7$, which have been obtained using Eqs. (1) and (2), where the horizontal axis represents the number of just one He or H atoms in the interstitial sites for the present study. Table 1 summarizes our

calculated formation energies of all these defect structures, as shown in Fig. 1, and compared to the other calculated data for only He-dopant, which have already been reported by L. Yang [2]. The doped-He atom prefers to occupy octahedral-interstitial site in $Y_2Ti_2O_7$ to tetrahedral-one, with resulting defect formation energies of $E_{defect}^{He\,in\,Y_2Ti_2O_7\,(octa.)}$=1.02 eV and $E_{defect}^{He\,in\,Y_2Ti_2O_7\,(tetra.)}$=1.59 eV, respectively, which are in good agreement with the other data within a little bit deviation of less than approximately 0.084 eV. The deviation may be caused by the differences of the set energy cut-off of 650 eV for this work and 500 eV for L. Yang, and the total calculation time of 72 hrs for this work and unknown time for L. Yang. On the other hand, the doped-H atom prefers to occupy tetrahedral-interstitial site to octahedral-one, with resulting defect formation energies of $E_{defect}^{H\,in\,Y_2Ti_2O_7\,(tetra.)}$=2.87 eV and $E_{defect}^{H\,in\,Y_2Ti_2O_7\,(octa.)}$=3.01 eV, respectively. In addition, the formation energies of H defects are much higher than those of He ones. The result indicates that He atoms can trap at interstitial sites in $Y_2Ti_2O_7$ easier than H.

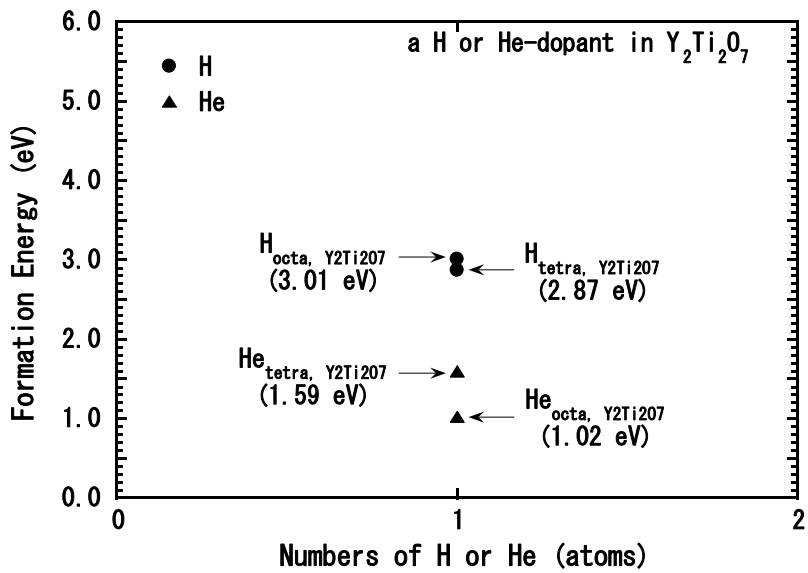

Figure 3. Calculated formation energies of (▲) He and (●) H in tetrahedral- and octahedral-interstitial sites in $Y_2Ti_2O_7$.

Table 1 Calculated formation energies of He and H tetrahedral- and octahedral-interstitial sites in $Y_2Ti_2O_7$, as compared to those of He defects which have been reported by L. Yang.

	Tetrahedral-interstitial site		Octahedral-interstitial site	
	$E_{defect}^{He\,in\,Y_2Ti_2O_7\,(tetra.)}$ [eV]	$E_{defect}^{H\,in\,Y_2Ti_2O_7\,(tetra.)}$ [eV]	$E_{defect}^{He\,in\,Y_2Ti_2O_7\,(octa.)}$ [eV]	$E_{defect}^{H\,in\,Y_2Ti_2O_7\,(octa.)}$ [eV]
This work	1.59	2.87	1.02	3.01
Theory by L. Yang [2]	1.51		0.94	

Figure 4 shows calculated formation energies of (a) He and (b) H defects in $Y_2Ti_2O_7$ compared to in Fe, in order to estimate the relative stability of He and H in $Y_2Ti_2O_7$ and Fe. The He atom energy in the octahedral site in $Y_2Ti_2O_7$ is much lower than the corresponding energy in tetrahedral-, octahedral-interstitial, and substitutional, sites in Fe, at 4.47, 4.67, and 2.23 eV, respectively. The calculated formation energy of a vacancy in Fe bulk, E^{v}_{defect}=2.08 eV, is less than the half of those of interstitial He. These results are consistent with DFT calculations of the reported ones [2, 5], as denoted in Table 2. In contrast, the H atom energy in tetrahedral-, octahedral-interstitial, or substitutional, sites in Fe, at 0.11, 0.24, and 0.41 eV, respectively, which are close to the reported ones [8, 10-12], is much lower than in $Y_2Ti_2O_7$. It is suggested from these results that just one He or H atom in NFAs prefers to occupy individual octahedral-interstitial sites in $Y_2Ti_2O_7$ and tetrahedral-interstitial sites in Fe, respectively. This calculation result indicates that the simultaneous He- and H-induced synergistic effect in void and bubble growths, dislocation bias, and swelling [18], in NFAs does not occur due to dispersion of the nanometer-sized oxide particles in Fe.

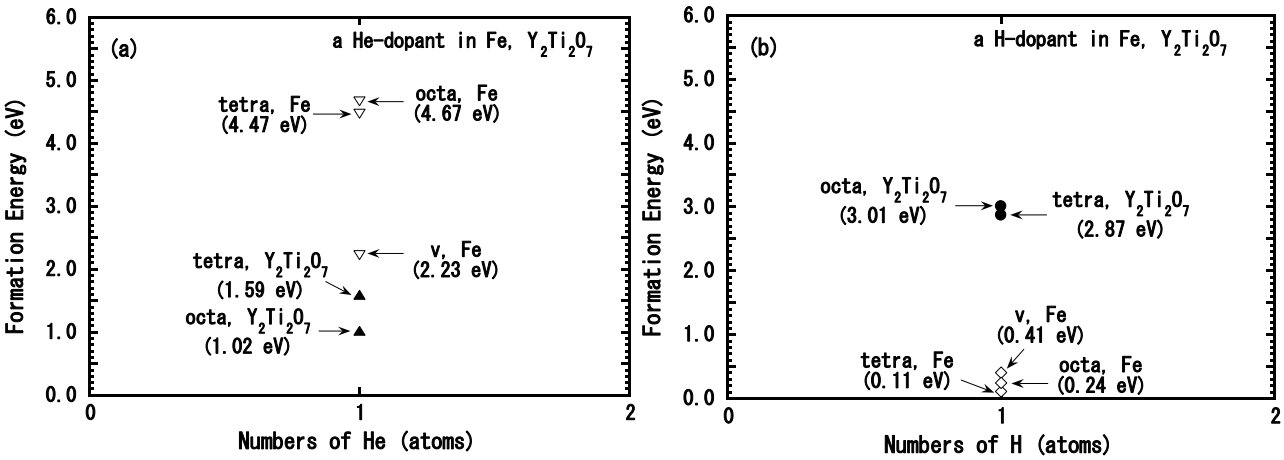

Figure 4. Calculated formation energies of (a) He and (b) H in $Y_2Ti_2O_7$ as compared to those in Fe.

Table 2 Calculated formation energies of He and H IN tetrahedral-, octahedral-interstitial, substitutional sites in Fe, as compared to the references.

	Tetrahedral-interstitial site		Octahedral-interstitial site		Substitutional site	
	$E_{defect}^{He\,in\,Fe\,(tetra.)}$ [eV]	$E_{defect}^{H\,in\,Fe\,(tetra.)}$ [eV]	$E_{defect}^{He\,in\,Fe\,(octa.)}$ [eV]	$E_{defect}^{H\,in\,Fe\,(octa.)}$ [eV]	$E_{defect}^{He\,in\,Fe\,(v)}$ [eV]	$E_{defect}^{H\,in\,Fe\,(v)}$ [eV]
This work	4.47	0.11	4.67	0.24	2.23	0.41
Theory by L. Yang [2]	4.63		4.83		2.28	
Theory by C. C. Fu [5]	4.40		4.58		2.09	
Theory by D. E. Jiang [8]		0.30		0.43		
Theory by S. K. Desai [10]		0.26		0.39		
Theory by W. A. Counts [12]		0.21		0.34		0.57
Experiment by F. Besenbacher [11]						0.63

REFERENCES

[1] G. R. Odette, M. J. Alinger, and B. D. Wirth, Annu. Rev. Mater. Res. 38, (2008), 471-503.
[2] L. Yang, Y. Jiang, G. R. Odette, T. Yamamoto, Z. Liu, and Y. Liu, J. Appl. Phys. 115, (2014), 143508.
[3] P. Erhart, J. Appl. Phys. 111, (2012), 113502.
[4] T. Seletskaia, Y. N. Osetsky, R. E. Stoller, and G. M. Stocks, Phys. Rev. Lett. 94 (2005) 046403.
[5] C. C. Fu and F. Willaime, Phys. Rev. B. 72, (2005,) 064117.
[6] J. M. Pruneda and E. Artacho, Phys. Rev. B 72, (2005), 085107.
[7] T. Seletskaia, Y. N. Osetsky, R. E. Stoller, and G. M. Stocks, J. Nucl. Mater., 351, (2006), 109-118.
[8] D. E. Jiang and E. A. Carter, Phys. Rev. B 70, (2004), 064102.
[9] E. J. Song, H. K. D. H. Bhadeshia, and D. W. Suh, Corrosion Science 77, (2013), 379-384.
[10] S. K. Desai, T. Neeraj, and P.A. Gordon, Acta Materialia, 58, (2010), 5363-5369.
[11] F. Besenbacher, S. M. Myers, P. Nordlander, and J. K. Nørskov, J. Appl. Phys. 61, (1987), 1788.
[12] W. A. Counts, C. Wolverton, and R. Gibala, Acta Materialia 58, (2010,) 4730-4741.
[13] M. L. Fullarton, R. E. Voskoboinikov, S. C. Middleburgh, J. Alloys Comp. 587, (2014), 794-799.
[14] G. Kresse and J. Hafner, Phys. Rev. B 47, (1993), 558.
[15] G. Kresse and J. Furthmüller, Phys. Rev. B 54 (1996) 11169.
[16] G. Herzberg, Molecular Spectra and Molecular Structure: Spectra of Diatomic Molecules, 2nd ed., Krieger, 1989.
[17] K. P. Huber and G. Hertzberg, Molecular Spectra and Molecular Structure IV: Constants of Diatomic Molecules (Van Norstrand Reinhold, New York, 1979).
[18] T. Tanaka, K. Oka, S. Ohnuki, S. Yamashita, T. Suda, S. Watanabe, E. Wakai, J. Nucl. Mater., 329-333, (2004), 294-298.